American Mineralogist, Volume 82, pages 61–68, 1997

The pressure behavior of clinozoisite and zoisite: An X-ray diffraction study

PAOLA COMODI AND PIER FRANCESCO ZANAZZI

Dipartimento di Scienze della Terra, Università di Perugia, Piazza Università, I-06100 Perugia, Italy

ABSTRACT

Compressibility data of clinozoisite and zoisite were measured by single-crystal X-ray diffraction in a diamond-anvil cell up to a pressure of about 50 kbar. In both polymorphs, the unit cell parameters varied linearly with pressure but in an anisotropic pattern: β_a = 2.1(1) × 10^{-4}, β_b = 2.8(1) × 10^{-4}, β_c = 3.3(1) × 10^{-4} $kbar^{-1}$ for clinozoisite, and β_a = 2.3(2) × 10^{-4}, β_b = 2.9(1) × 10^{-4}, β_c = 3.7(2) × 10^{-4} $kbar^{-1}$ for zoisite. The principal coefficients of the strain ellipsoid of clinozoisite are β_1 = 2.0 × 10^{-4}, β_2 = 2.7 × 10^{-4}, β_3 = 3.3 × 10^{-4} $kbar^{-1}$; β_1 and β_3 were symmetrically oriented in the (010) plane with an angle of about 12° between β_1 and the *a* axis, whereas β_2 coincides with the *b* axis. Bulk moduli calculated as the reciprocal of cell-volume compressibility were 1300(20) kbar for the monoclinic and 1140(20) for the orthorhombic polymorph. K_0, determined by fitting the unit-cell parameters with a third-order Birch-Murnaghan equation of state, was 1270(45) kbar, with K' = 0.5(2) for clinozoisite and 1020(65) kbar with K' = 4.8(4) for zoisite.

Structural refinements of clinozoisite performed at 0.5, 19.4, and 42 kbar, and also under ambient conditions, showed that the compression mechanism included both shrinking of the polyhedra (i.e., octahedra and Ca polyhedra) and tilting of the Si_2O_7 group, with reduction of the Si-O-Si angle. The different effect of these mechanisms explains the anisotropic compressional pattern in clinozoisite and the similar behavior observed in the two polymorphs.

Comparison of high-pressure and high-temperature data for clinozoisite showed that a given increase in pressure produced structural effects very similar to those seen after a proportional decrease in temperature. The calculated volume-expansivity–to–compressibility ratio of 38 bar/K indicates that the cell volume of clinozoisite remains unchanged with geothermal gradients of about 10 °C/km. The crystallographic data support the results of experimental petrology in indicating that epidote is a good candidate for transporting H_2O in down-going subduction slabs.

INTRODUCTION

Clinozoisite and zoisite are the Fe-poor members of the epidote group. They crystallize in either orthorhombic (zoisite, space group *Pnma*) or monoclinic (clinozoisite, space group $P2_1/m$) forms with the formula $Ca_2Al_{3-p}Fe_pSi_3O_{12}OH$, where p is <0.04 (Kvick et al. 1988), zoisite having a more restricted chemical range than clinozoisite. Dollase (1968) determined the structures of zoisite and clinozoisite and showed that the structure of zoisite could be related only approximately by a diagonal glide twin operation on (100) to the monoclinic cell, as previously proposed by Ito (1950). On the basis of transmission electron microscopy observations, Ray et al. (1986) described a polytypical relationship between the clinozoisite and zoisite structures: A displacement by ¼[001] on (001) planes between clinozoisite unit-cell modules yields the zoisite structure. The polytypes can be interchanged by introducing a shear between the various stacking modules.

The essential features of the epidote structure are chains of edge-sharing octahedra parallel to the *b* axis. The chains are connected by both single tetrahedra (SiO_4) and pairs of tetrahedra (Si_2O_7). Although in clinozoisite there are two types of chains, one with only M2 octahedra and the other with M1 octahedra and M3 octahedra attached on alternate sides along the chain extension, in zoisite the *n*-glide "twin" operation produces only one kind of chain. Large cavities are formed where Ca atoms are hosted.

Zoisite and clinozoisite are relatively common constituents of rocks of the epidote-amphibole facies and also occur in both hydrothermal systems and high-*P* eclogite facies terrains. The stability relationships between the two forms are not completely known. Ackermand and Raase (1973) considered that zoisite was the stable phase at low *T*, whereas Jenkins et al. (1983) showed that it was the stable form relative to clinozoisite at 555 °C for Fe-free compositions. Prunier and Hewitt (1985), studying the coexisting phases in the Fe-bearing system, showed that zoisite is the stable high-*T*, Fe-poor phase.

0003–004X/97/0102–0061$05.00

Recent experimental studies (Schreyer 1988; Schmidt and Poli 1994; Ulmer et al. 1994; Pawley and Wood 1995) have shown that zoisite and clinozoisite, together with other hydrous phases such as antigorite, lawsonite, chloritoid, talc, staurolite, and phengite, are good candidates for the transport of H_2O to pressures higher than that of the amphibole stability field. In particular, Poli and Schmidt (1995) showed that, in andesitic rocks, amphibole disappears between 2.4 and 2.6 GPa, forming lawsonite at $T < 630$ °C and zoisite and clinozoisite at $T > 630$ °C. Thus, zoisite and clinozoisite are expected to carry H_2O beyond the amphibole stability field, with geothermal gradients higher than those possible for lawsonite, to depths of 100–120 km, where epidote breaks down.

To determine H_2O storage and release in subduction zones, it is necessary to know the stability of these hydrous phases within the slab and mantle wedge. Both compressibility and thermal expansion data are required to calculate thermodynamic data such as the enthalpy of formation of a phase, ΔH_f, and its behavior in reactions at high *P* and *T*. Recently, thermal expansion and compressibility of clinozoisite and zoisite were determined by energy-dispersive powder X-ray diffraction by Pawley et al. (1996) and Holland et al. (1996). In spite of the similar features of the atomic arrangement of the two polymorphs, their reported compressibility values are inexplicably very different. The aim of this paper, reporting and comparing the compressibilities of clinozoisite and zoisite on the basis of single-crystal methods, is to contribute to a more accurate definition of the equations of state of these phases. Moreover, structural refinement of clinozoisite at various pressures up to about 50 kbar provides information on the compression mechanisms of the epidote structure.

Experimental methods

The samples used for this work included a zoisite from Val Passiria, South Tyrol (Italy; sample no. 10265-G of the Mineralogy Museum of Florence University), with composition $Ca_2Al_2(Al_{0.9}Fe_{0.1})Si_3O_{12}OH$, and clinozoisite from Chiampernotto, Val d'Alba (Italy), with composition $Ca_2Al_2(Al_{0.78}Fe_{0.22})Si_3O_{12}OH$. The latter sample corresponds to the CH sample studied by Bonazzi and Menchetti (1995). Both samples had nearly identical compositions and near end-member compositions.

Diffraction data were collected under ambient conditions on a four-circle Philips PW1100 diffractometer from a clinozoisite crystal with dimensions 0.12 × 0.10 × 0.06 mm using graphite-monochromatized Mo*K*α radiation (λ = 0.7107 Å). For structural refinement, 2758 integrated intensities from two equivalent sets with indices ±*hkl* and ±*hk̄l* (up to 35° ϑ) were collected (Table 1). An empirical absorption correction based on the method of North et al. (1968) was applied: Transmission factors were in the range 1.0–0.9. After merging of equivalent reflections (R_{eq} = 3.3%), 1210 independent reflections with intensities $>3\sigma_I$ were obtained. Anisotropic refinement in space group $P2_1/m$ was performed using the SHELX76 program (Sheldrick 1976). On the basis of the chemical data, a substitution of 0.2 atoms of Fe^{3+} for Al was considered in the M3 site, and the occupancy of Fe vs. Al was refined. The final value of Fe occupancy was 0.21 ± 0.01, in good agreement with the analytical results. In the late stages of refinement, one peak in the Fourier-difference map was assigned to the H atom of the OH group. Further refinement cycles, including the H-atom contribution, improved the agreement index and resulted in a final *R* of 2.1% for 123 parameters. Final atomic coordinates and displacement parameters are listed in Table 2. Observed and calculated structure factors are listed in Table 3.[1]

Table 1. Data collection and refinement details

	Zoisite	Clinozoisite			
P (kbar)	0.001	0.001	0.5	19.4	42
No. refl.	3549	2758	1298	1110	1100
No. unique ($I > 3\sigma_I$)	1160	1210	392	363	417
No. par.	119	123	56	56	56
R_{eq} (%)	2.3	3.3	4.6	3.9	4.8
R^* (%)	2.0	2.1	5.7	4.8	6.9
θ range (°)	35	35	35	35	35
scan type	ω	ω	ω	ω	ω
scan width (°)	2.5	2.5	3	3	3
scan speed (°/sec)	0.04–0.08	0.04–0.08	0.04	0.04	0.04
GoF**	0.89	0.51	1.35	1.21	2.16

Note: Variable scan speed was used to improve counting statistics.
* $R(F) = \Sigma||F_o| - |F_c||/\Sigma|F_o|$.
** GoF = $[\Sigma w_i(F_o - F_c)^2/(N - P)]^{1/2}$, with $w_i = 1/\sigma_F^2$.

Intensity data for the refinement of zoisite were measured under the same conditions as for clinozoisite from a crystal with dimensions 0.13 × 0.10 × 0.50 mm. A total of 3549 reflections from the reciprocal lattice octants *hkl*, *hk̄l*, and *hkl̄* were collected and merged to give 1160 independent reflections with $I > 3\sigma$ (R_{eq} = 2.3%). The anisotropic refinement in space group *Pnma* converged to a final *R* value of 2.0% for 119 parameters. In the M2 site a substitution of 12% Fe for Al was indicated, in agreement with the chemical analysis. Final atomic coordinates and atomic displacement parameters are listed in Table 2. Observed and calculated structure factors are listed in Table 3.[1]

A Merrill-Bassett diamond-anvil cell (DAC) with ⅛ carat diamonds was used for the high-*P* study. An Sm^{2+}:BaFCl powder for *P* calibration (Comodi and Zanazzi 1993) and a 16:3:1 methanol:ethanol:water mixture as a pressure medium were introduced into the DAC together with the sample. *P* was monitored by measuring the wavelength shift of the Sm^{2+} line excited by a 100 mw argon laser and detected by a 100 cm Jarrell-Ash optical spectrometer. The precision of the *P* measurements was 0.5 kbar. Steel foil, 250 μm thick, with a hole 300 μm in diameter, was used as gasket material. The lattice param-

[1] A copy of Table 3 may be ordered as Document AM-97-631 from the Business Office, Mineralogical Society of America, 1015 Eighteenth Street NW, Suite 601, Washington, DC 20036. Please remit $5.00 in advance for the microfiche.

TABLE 2. Atomic fractional coordinates and anisotropic displacement factors (Å²) of clinozoisite and zoisite at room pressure

Atom	*x*	*y*	*z*	U_{11}	U_{22}	U_{33}	U_{23}	U_{13}	U_{12}
Clinozoisite									
A1	0.7606(1)	¾	0.1546(1)	0.0103(2)	0.0088(2)	0.0079(2)	0	0.0056(2)	0
A2	0.6068(1)	¾	0.4235(1)	0.0098(2)	0.0146(2)	0.0070(2)	0	0.0030(2)	0
Si1	0.3385(1)	¾	0.0481(1)	0.0040(2)	0.0045(3)	0.0041(3)	0	0.0011(2)	0
Si2	0.6791(1)	¼	0.2752(1)	0.0046(3)	0.0047(3)	0.0040(3)	0	0.0010(2)	0
Si3	0.1826(1)	¾	0.3164(1)	0.0045(3)	0.0048(3)	0.0036(3)	0	0.0015(2)	0
M1	0	0	0	0.0050(3)	0.0042(3)	0.0047(3)	−0.0004(2)	0.0009(2)	−0.0002(2)
M2	0	0	½	0.0050(3)	0.0041(3)	0.0051(3)	0.0000(2)	0.0011(2)	0.0001(2)
M3	0.2893(1)	¼	0.2239(1)	0.0043(2)	0.0065(3)	0.0055(2)	0	0.0011(2)	0
O1	0.2344(1)	0.9964(2)	0.0446(1)	0.0058(5)	0.0065(5)	0.0097(5)	0.0009(4)	0.0030(4)	0.0012(4)
O2	0.3011(1)	0.9852(2)	0.3522(1)	0.0084(5)	0.0079(5)	0.0066(5)	−0.0014(4)	0.0034(4)	−0.0025(4)
O3	0.7893(1)	0.0129(2)	0.3454(1)	0.0064(5)	0.0048(5)	0.0094(5)	−0.0003(4)	−0.0012(4)	0.0005(4)
O4	0.0543(2)	¼	0.1316(2)	0.0066(6)	0.0050(7)	0.0049(6)	0	0.0017(5)	0
O5	0.0396(2)	¾	0.1432(2)	0.0068(6)	0.0059(7)	0.0043(6)	0	0.0019(5)	0
O6	0.0610(2)	¾	0.4015(2)	0.0081(6)	0.0056(7)	0.0066(7)	0	0.0048(5)	0
O7	0.5167(2)	¾	0.1782(2)	0.0060(6)	0.0114(7)	0.0072(7)	0	0.0006(5)	0
O8	0.5122(2)	¼	0.2976(2)	0.0098(7)	0.0133(7)	0.0139(7)	0	0.0084(6)	0
O9	0.6384(2)	¼	0.1033(2)	0.0236(8)	0.0209(9)	0.0080(7)	0	0.0104(6)	0
O10	0.0770(2)	¼	0.4246(2)	0.0078(6)	0.0064(7)	0.0054(6)	0	0.0038(5)	0
H	0.053(2)	¼	0.351(2)	0.050(2)					
Zoisite									
A1	0.3668(1)	¼	0.4373(1)	0.0074(3)	0.0098(3)	0.0069(2)	0	0.0009(2)	0
A2	0.4518(1)	¼	0.1150(1)	0.0125(3)	0.0110(3)	0.0077(2)	0	−0.0001(2)	0
Si1	0.0813(1)	¼	0.1055(1)	0.0039(3)	0.0043(3)	0.0053(3)	0	−0.0006(3)	0
Si2	0.4105(1)	¾	0.2824(1)	0.0044(3)	0.0049(3)	0.0051(3)	0	−0.0003(3)	0
Si3	0.1600(1)	¼	0.4357(1)	0.0049(4)	0.0043(4)	0.0047(3)	0	0.0005(2)	0
M1	0.2497(1)	0.9970(1)	0.1897(1)	0.0047(3)	0.0040(3)	0.0060(3)	−0.0003(2)	0.0002(2)	−0.0001(2)
M2	0.1055(1)	¾	0.3004(1)	0.0035(4)	0.0061(4)	0.0074(3)	0	−0.0005(2)	0
O1	0.1307(1)	−0.0006(2)	0.1453(1)	0.0059(6)	0.0055(7)	0.0107(6)	−0.0003(5)	−0.0019(5)	0.0003(5)
O2	0.1011(1)	0.0137(2)	0.4309(1)	0.0073(7)	0.0078(7)	0.0083(6)	−0.0006(5)	0.0016(5)	−0.0019(5)
O3	0.3587(1)	0.9897(2)	0.2450(1)	0.0067(7)	0.0042(7)	0.0118(6)	0.0001(5)	−0.0017(5)	−0.0004(4)
O4	0.2193(1)	¾	0.3004(2)	0.0076(9)	0.0034(8)	0.0082(8)	0	−0.0009(7)	0
O5	0.2275(1)	¼	0.3119(2)	0.0062(9)	0.0047(8)	0.0050(8)	0	0.0010(6)	0
O6	0.2718(1)	¾	0.0600(2)	0.0045(9)	0.0073(9)	0.0050(8)	0	−0.0009(6)	0
O7	0.9916(1)	¼	0.1639(2)	0.006(1)	0.0100(9)	0.0128(9)	0	0.0011(8)	0
O8	0.9960(1)	¾	0.2952(2)	0.008(1)	0.0126(9)	0.0141(9)	0	−0.0026(8)	0
O9	0.4211(1)	¾	0.4431(2)	0.019(1)	0.023(1)	0.0073(9)	0	−0.0002(8)	0
O10	0.2682(1)	¼	1.0754(2)	0.013(1)	0.0058(9)	0.0063(8)	0	0.0014(8)	0
H	0.263(3)	¼	0.976(7)	0.050					

TABLE 4. Unit-cell parameters of clinozoisite and zoisite as a function of pressure

P (kbar)	*a* (Å)	*b* (Å)	*c* (Å)	β (°)	V (Å³)
Clinozoisite					
0.001	8.870(1)	5.592(1)	10.144(2)	115.4(2)	454.3(2)
0.5	8.874(4)	5.593(3)	10.139(5)	115.4(4)	454.6(7)
9.2	8.858(4)	5.578(3)	10.103(5)	115.4(4)	450.9(7)
19.4	8.840(4)	5.566(3)	10.070(5)	115.5(4)	447.2(7)
27.7	8.822(4)	5.556(3)	10.050(5)	115.4(4)	445.0(7)
31.4	8.810(4)	5.550(3)	10.037(5)	115.4(4)	443.3(7)
38.0	8.800(4)	5.534(3)	10.011(5)	115.2(5)	441.1(7)
42.0	8.793(4)	5.526(3)	9.996(5)	115.3(5)	439.1(7)
13.3*	8.845(4)	5.575(3)	10.106(5)	115.5(4)	449.8(7)
46.0*	8.784(5)	5.518(3)	9.993(6)	115.2(5)	438.3(7)
51.0*	8.780(10)	5.515(7)	9.987(10)	115.4(7)	436.8(15)
Zoisite					
0.001	16.212(3)	5.555(1)	10.034(2)		903.6(4)
2.7	16.186(9)	5.554(2)	10.033(5)		901.9(12)
7.0	16.174(10)	5.544(2)	10.001(5)		896.8(12)
18.4	16.131(10)	5.528(2)	9.952(5)		887.4(13)
25.2	16.123(15)	5.519(2)	9.935(5)		884.0(14)
15.3*	16.137(10)	5.529(2)	9.974(5)		889.9(12)
32.5*	16.087(10)	5.504(2)	9.920(5)		878.3(12)
36.0*	16.055(15)	5.498(2)	9.905(5)		874.3(14)

Note: Standard deviations are in parentheses. The *P* uncertainty is about 0.5 kbar.

* Second sample examined for each polymorph.

eters of two crystals, selected from the same sample, were determined at increasing pressure between 1 bar and 51 kbar for clinozoisite and between 1 bar and 36 kbar for zoisite (Table 4) by the least-squares method and the positions of about 30 accurately centered Bragg reflections in the range 10–30° 2ϑ.

Intensity data for clinozoisite were collected at 19.4 and 42 kbar up to 35°ϑ, adopting nonbisecting geometry (Denner et al. 1978) and a 2.5° ω scan mode; data were corrected for pressure-cell absorption by an experimental attenuation curve (Finger and King 1978). Systematic errors may be introduced by comparison of refinement results and cell parameters obtained from reflections belonging to the whole reciprocal lattice when measured outside the DAC, with results obtained from reflections measured within the DAC, where access to reciprocal space is limited (Glinnemann 1990). Therefore, the same set of intensity data was collected at 0.5 kbar from the same crystal and using the same procedure.

Intensity data were analyzed with a digital procedure (Comodi et al. 1994) that involved multiplying the Fourier-transformed data of the profile by a low-pass filter and then back-transforming the data. Reflections were visually inspected to eliminate errors caused by the overlap

Table 5. Atomic fractional coordinates and isotropic displacement factors (Å²) of clinozoisite

Atom	*x*	*y*	*z*	*U*
A1	0.7604(4)	¾	0.1542(6)	0.0098(5)
	0.7611(4)	¾	0.1554(6)	0.0081(4)
	0.7592(4)	¾	0.1529(3)	0.0101(8)
A2	0.6072(4)	¾	0.4236(7)	0.0136(5)
	0.6069(4)	¾	0.4255(6)	0.0110(5)
	0.6048(4)	¾	0.4276(3)	0.0097(8)
Si1	0.3388(5)	¾	0.0481(8)	0.0057(6)
	0.3398(5)	¾	0.0482(8)	0.0048(6)
	0.3410(5)	¾	0.0508(5)	0.0049(9)
Si2	0.6788(5)	¼	0.2753(8)	0.0058(6)
	0.6797(5)	¼	0.2755(8)	0.0065(6)
	0.6800(5)	¼	0.2751(5)	0.0071(9)
Si3	0.1814(5)	¾	0.3155(8)	0.0055(6)
	0.1821(5)	¾	0.3164(8)	0.0042(6)
	0.1837(4)	¾	0.3170(4)	0.0048(9)
M1	0	0	0	0.0057(7)
	0	0	0	0.0060(6)
	0	0	0	0.006(1)
M2	0	0	½	0.0055(7)
	0	0	½	0.0058(6)
	0	0	½	0.005(1)
M3	0.2891(5)	¼	0.2227(7)	0.0074(6)
	0.2904(5)	¼	0.2243(7)	0.0062(6)
	0.2913(4)	¼	0.2237(4)	0.0019(8)
O1	0.233(1)	0.9953(7)	0.042(2)	0.008(1)
	0.2353(9)	0.9977(7)	0.045(1)	0.006(1)
	0.2354(8)	0.998(2)	0.0455(8)	0.007(2)
O2	0.304(1)	0.9840(7)	0.355(2)	0.008(1)
	0.304(1)	0.9863(7)	0.355(2)	0.008(1)
	0.3037(8)	0.985(2)	0.3532(7)	0.004(2)
O3	0.790(1)	0.0128(8)	0.346(2)	0.010(1)
	0.790(1)	0.0128(8)	0.347(2)	0.009(1)
	0.7911(9)	0.014(3)	0.3439(9)	0.014(2)
O4	0.052(1)	¼	0.130(2)	0.007(2)
	0.052(1)	¼	0.130(2)	0.006(1)
	0.053(1)	¼	0.135(1)	0.006(2)
O5	0.037(1)	¾	0.140(2)	0.009(2)
	0.039(1)	¾	0.142(2)	0.005(1)
	0.039(1)	¾	0.142(1)	0.003(2)
O6	0.062(1)	¾	0.403(2)	0.005(1)
	0.063(1)	¾	0.404(2)	0.008(1)
	0.063(1)	¾	0.404(1)	0.007(2)
O7	0.519(2)	¾	0.181(2)	0.012(2)
	0.519(1)	¾	0.181(2)	0.009(1)
	0.516(1)	¾	0.182(1)	0.007(2)
O8	0.513(1)	¼	0.299(2)	0.010(2)
	0.513(1)	¼	0.300(2)	0.007(2)
	0.516(1)	¼	0.306(1)	0.013(3)
O9	0.640(2)	¼	0.106(2)	0.019(2)
	0.634(2)	¼	0.100(2)	0.018(2)
	0.631(1)	¼	0.100(1)	0.015(3)
O10	0.079(1)	¼	0.426(2)	0.008(2)
	0.078(1)	¼	0.425(2)	0.004(1)
	0.078(1)	¼	0.422(1)	0.012(3)

Note: For each entry the first, second, and third values refer to 0.5, 19.4, and 42 kbar refinements, respectively.

of diffraction effects from various parts of the diamond cell or by shadowing by the gasket, and they were merged to an independent data set.

The structure was refined in space group $P2_1/m$, with individual isotropic atomic displacement parameters, using the SHELX76 program. Details of the refinements are listed in Table 1. Final fractional atomic positions and displacement parameters are shown in Table 5. Observed and calculated structure factors are listed in Table 3.[1]

Results and discussion

Clinozoisite and zoisite: Structures at room pressure and temperature

The room-*P* structural refinement for clinozoisite (Table 2) is in perfect agreement with the refinement on the same sample performed by Bonazzi and Menchetti (1995) and confirms the general features of the clinozoisite structure described by Dollase (1968): Although the M1 and M2 octahedra are completely occupied by Al atoms, the main substitution of Fe for Al involves the M3 octahedral site, distinctly different in size and shape from the octahedral chain sites M1 and M2. The occupancy refinement was consistent with the chemical analysis.

The H atom was uniquely located on the O10 atom (O10-H = 0.69 Å). It was involved in a bent hydrogen bond with the O4 atom (O4-O10 = 2.89 Å), as shown by a neutron diffraction study at 15 K (Kvich et al. 1988).

The refinement results for zoisite were in good agreement with the results of Dollase (1968). The fractional atomic coordinates given in Table 2, based on a greater number of observations and with a better agreement factor, represent a more reliable determination of the orthorhombic epidote structure with respect to other results reported in the literature. Because the details of the zoisite structure are beyond the scope of this work, they will not be discussed further.

Compressibility

Variations in unit-cell dimensions with *P* are shown in Figure 1 and Table 4. No variation was observed among trends of different crystals of the same sample. The lattice parameters of both polymorphs decreased linearly over the *P* range examined; the average compressibility coefficients, obtained by linear regression, are shown in Table 6. In clinozoisite, the β angle did not change significantly with increasing *P*. The compressional patterns of both clinozoisite and zoisite were very similar: With respect to unit-cell edges, compressibilities were similar in both value and orientation. In both minerals the largest variations occurred along the *c* axis, the ratios among compressibility coefficients being $\beta_a:\beta_b:\beta_c$ = 1:1.33:1.57 for clinozoisite and $\beta_a:\beta_b:\beta_c$ = 1:1.26:1.61 for zoisite. However, because the strain ellipsoid must be aligned by symmetry with the unit-cell axes in zoisite but may vary in clinozoisite, deformation in the two polymorphs can be more correctly assessed by the comparison of the two strain ellipsoids. The main linear compression coefficients of clinozoisite and their orientation in relation to crystallographic axes were determined with the STRAIN program (Ohashi 1982) and are given in Table 6.

The average main compressibility coefficients of clinozoisite are $\beta_1 = 2.0(1) \times 10^{-4}$, $\beta_2 = 2.7(1) \times 10^{-4}$, $\beta_3 = 3.3(1) \times 10^{-4}$ kbar^{-1}. Principal axis β_2 is parallel to *b*, whereas the angles between principal axis β_1 and the *a* axis and between β_3 and the *c* axis were ~12°. As a consequence, the orientation of the strain ellipsoid (Fig. 2) was symmetric with respect to the *a* and *c* axes, i.e., the

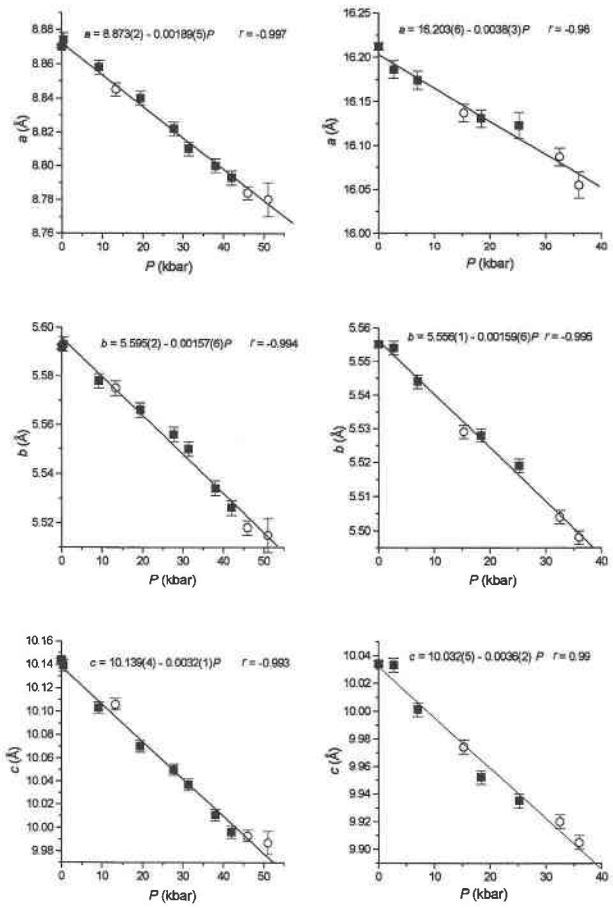

FIGURE 1. Compression of lattice parameters of clinozoisite (**left**) and zoisite (**right**). Closed squares and open circles represent two samples examined for each mineral.

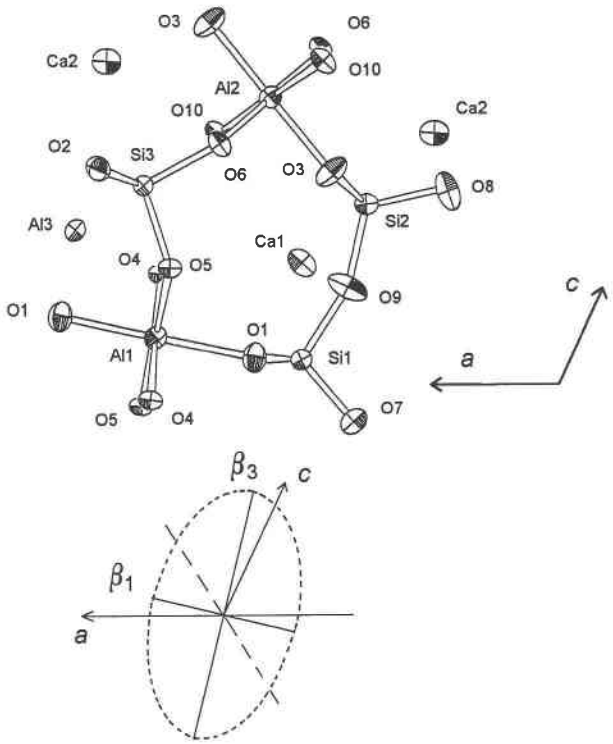

FIGURE 2. The (010) projection of the clinozoisite structure (**top**; modified from Gabe et al. 1973), and the (010) section of the strain ellipsoid (**bottom**).

two bisectrices of the monoclinic β angle between *a* and *c*, and that between $\beta_1$and β_3, coincided. Catti et al. (1988), analyzing the thermal behavior of a strontian piemontite, observed a thermal strain ellipsoid oriented in exactly the same way: Although α_2 coincided with the *b* axis, the smallest and the largest principal coefficients of thermal expansion, α_1 and α_3, were oriented symmetrically with respect to the *a* and *c* axes. Schlenker et al. (1978) showed that symmetric orientation of the strain tensor is observed when the monoclinic β angle does not change with strain.

The isothermal linear bulk moduli, calculated as the reciprocals of volume-cell compressibility, were 1300(20) kbar for clinozoisite and 1140(20) kbar for zoisite. Figure 3 shows the difference between the volume compressibility of the two polymorphs.

Bulk modulus K_0 and its *P* derivative *K'*, determined by fitting the unit-cell parameters with a third-order Birch-Murnaghan equation of state using the program BIRCH (Ross and Webb 1990), were 1270(45) kbar and $K' = 0.5(2)$ for clinozoisite, and 1020(65) kbar and $K' = 4.8(4)$ for zoisite. The values for *K'* were approximated because of the small *P* range investigated. The bulk modulus values compare well with those measured in other sorosilicates, e.g., in lawsonite $K_0 = 1100$ kbar (Comodi and Zanazzi 1996).

On the whole, the bulk compressibilities of the two polymorphs are similar, as expected from their structural and chemical similarities. Comparison of the anisotropies of their compressibility patterns, calculated using the $2(\beta_3 - \beta_1)/(\beta_3 + \beta_1)$ ratio proposed by Catti et al. (1988),

TABLE 6. Linear compressibility coefficients for clinozoisite and zoisite

	Cell-edge compressibilities ($\times 10^{-4}$ kbar^{-1})			Principal strain coefficients ($\times 10^{-4}$ kbar^{-1})			Orientation of principal coefficients [angle (°) with respect to axes] *a*	*b*	*c*
	β_a	β_b	β_c	β_1	β_2	β_3	β_1	β_2	β_3
clinozoisite	2.1(1)	2.8(1)	3.3(1)	2.0(1)	2.7(1)	3.3(2)	12	≡*b*	12
zoisite	2.3(2)	2.9(1)	3.7(2)	2.3(2)	2.9(1)	3.7(2)	≡*a*	≡*b*	≡*c*

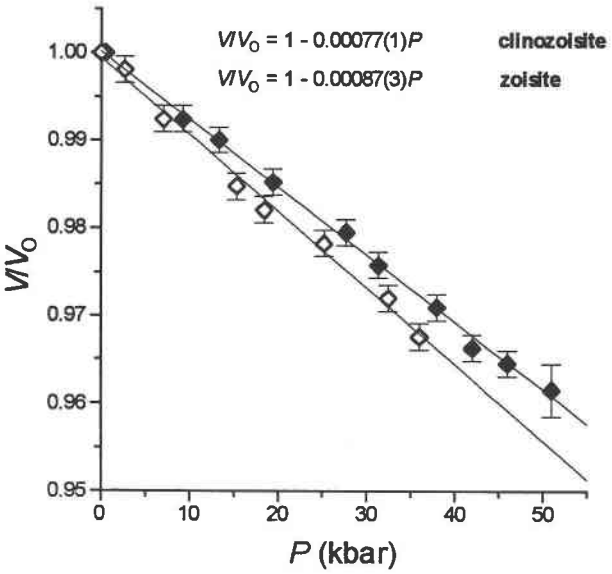

FIGURE 3. Cell volumes of clinozoisite (closed diamonds) and zoisite (open diamonds) at various pressures, normalized to room-condition values.

shows that the anisotropy of clinozoisite, 0.49(6), and that of zoisite, 0.46(10), are equal within their standard deviations. Even if we had not collected structural data of zoisite at high *P*, we could qualitatively explain the strong similarity in compressibility pattern by comparing the two well-known structures.

From powder diffraction data collected using synchrotron radiation and the energy-dispersive method, Holland et al. (1996) measured isothermal bulk moduli of 1540(60) and 2790(90) kbar for clinozoisite and zoisite, respectively. The agreement with our data is poor, especially for zoisite, the compressibility of which is unexpectedly low in comparison with that of clinozoisite. As discussed by Reynard et al. (1996), discrepancies between high-*P* single-crystal and powder data have been observed and can probably be ascribed to nonhydrostatic stresses and *P* gradients or to differences in the method of *P* calibration.

Clinozoisite: Structural evolution with pressure

Comparison of the three structural refinements at 0.5, 19.4, and 42 kbar resulted in several observations. First, the M1 and M2 octahedra showed rigid behavior with *P*; the M1 octahedron was incompressible, and the bulk modulus of the M2 octahedron was 1500(200) kbar. In effect, the ⟨M1-O⟩ and ⟨M2-O⟩ distances (Table 7) were the shortest measured for Al octahedra and were smaller than the sum of the ionic radii (1.915 Å; Shannon 1976).

The shared edges of the octahedra forming chains parallel to the *b* axis were shorter than the unshared ones because of Al-Al repulsion (Table 8). With increasing *P*, the octahedra became more regular: Unshared edges decreased, whereas shared ones remained unchanged over the *P* range investigated. In particular, the reduction of the O4-O5 unshared edge of the M1 octahedron, from 2.805 Å at 0.5 kbar to 2.768 Å at 42 kbar, and that of the O6-O10 unshared edge of the M2 octahedron (from

TABLE 7. Bond distances (Å) and polyhedral volumes (Å³) in clinozoisite at different pressures

P (kbar)	0.001	0.5	19.4	42
T1-O1 × 2	1.650(1)	1.651(5)	1.653(4)	1.646(12)
T1-O7	1.564(2)	1.591(18)	1.575(16)	1.531(10)
T1-O9	1.634(1)	1.653(10)	1.611(10)	1.627(10)
⟨T1-O⟩	1.625	1.636	1.623	1.613
VT1	2.192(4)	2.24(4)	2.18(3)	2.14(4)
T2-O3 × 2	1.619(1)	1.625(8)	1.619(8)	1.597(13)
T2-O8	1.591(2)	1.591(7)	1.601(7)	1.596(11)
T2-O9	1.622(2)	1.598(17)	1.630(16)	1.614(12)
⟨T2-O⟩	1.613	1.610	1.617	1.601
VT2	2.150(6)	2.14(4)	2.17(4)	2.10(4)
T3-O2 × 2	1.624(1)	1.638(7)	1.636(6)	1.614(12)
T3-O5	1.667(2)	1.689(18)	1.662(15)	1.663(10)
T3-O6	1.646(2)	1.648(10)	1.636(10)	1.638(11)
⟨T3-O⟩	1.640	1.653	1.643	1.632
VT3	2.246(6)	2.30(4)	2.26(4)	2.21(4)
M1-O1 × 2	1.928(1)	1.92(1)	1.928(5)	1.919(6)
M1-O4 × 2	1.848(1)	1.84(1)	1.831(10)	1.843(7)
M1-O5 × 2	1.936(1)	1.92(1)	1.919(11)	1.902(7)
⟨M1-O⟩	1.904	1.89	1.893	1.888
VM1	9.12(1)	8.95(13)	8.95(12)	8.90(9)
M2-O3 × 2	1.854(1)	1.847(13)	1.830(12)	1.830(8)
M2-O6 × 2	1.926(10)	1.922(8)	1.911(8)	1.895(7)
M2-O10 × 2	1.859(1)	1.857(7)	1.856(6)	1.854(7)
⟨M2-O⟩	1.880	1.875	1.866	1.860
VM2	8.80(1)	8.73(12)	8.60(12)	8.53(10)
M3-O1 × 2	2.190(1)	2.20(1)	2.168(10)	2.143(10)
M3-O2 × 2	1.944(10)	1.97(1)	1.938(9)	1.926(11)
M3-O4	1.882(2)	1.90(1)	1.905(11)	1.896(10)
M3-O8	1.788(2)	1.80(1)	1.775(9)	1.786(10)
⟨M3-O⟩	1.990	2.01	1.982	1.970
VM3	10.19(2)	10.4(2)	10.1(1)	9.9(1)
A1-O7	2.277(2)	2.271(8)	2.266(7)	2.279(10)
A1-O3 × 2	2.355(1)	2.364(12)	2.343(11)	2.322(11)
A1-O1 × 2	2.485(2)	2.468(10)	2.472(10)	2.439(10)
A1-O5	2.526(2)	2.517(7)	2.520(6)	2.513(10)
A1-O6	2.764(2)	2.781(16)	2.764(16)	2.768(10)
A1-O9 × 2	2.963(2)	2.958(4)	2.964(4)	2.945(4)
⟨A1-O⟩	2.575	2.572	2.568	2.552
VA1	27.43(6)	27.2(3)	27.0(3)	26.5(3)
A2-O7	2.263(2)	2.234(19)	2.237(18)	2.237(10)
A2-O2 × 2	2.814(1)	2.796(7)	2.790(7)	2.750(9)
A2-O10	2.554(1)	2.538(10)	2.533(10)	2.539(10)
A2-O3 × 2	2.552(10)	2.547(6)	2.555(5)	2.587(11)
A2-O2 × 2	2.537(1)	2.525(10)	2.485(10)	2.464(10)
A2-O8 × 2	3.038(1)	3.033(7)	3.021(7)	2.985(4)
⟨A2-O⟩	2.670	2.657	2.647	2.635
VA2	42.66(5)	42.1(4)	41.4(4)	40.7(4)

TABLE 8. Variation with *P* of selected distances (Å) and angles (°) in clinozoisite

P (kbar)	0.001	0.5	19.4	42
Si1···Si2	3.216(2)	3.215(7)	3.189(6)	3.183(7)
Si1-O9-Si2	161.9(1)	162.9(7)	160.1(6)	158.1(7)
M1*	2.552(2)	2.54(1)	2.53(1)	2.54(1)
M1**	2.762(2)	2.74(1)	2.76(1)	2.73(1)
M2*	2.543(3)	2.53(1)	2.53(1)	2.53(1)
M2**	2.680(2)	2.68(1)	2.66(1)	2.65(1)
M3*	2.560(1)	2.57(1)	2.56(1)	2.56(1)
M3**	2.854(2)	2.88(1)	2.84(1)	2.82(1)

* Mean lengths of shared O-O edges.
** Mean lengths of unshared O-O edges.

2.804 Å to 2.768 Å), oriented nearly along the *b* axis, reduced the *b* lattice parameter.

In the M3 octahedron, Fe ↔ Al substitution reduced O-O repulsions by increasing octahedral dimensions, so its compressibility was higher than that of one completely filled by Al [K_{M3} = 1000(200) kbar]. The octahedron compressed anisotropically, becoming more regular with *P*: The four longer distances, M3-O1 and M3-O2 (Table 6), were reduced in length, whereas the two shorter distances, M3-O4 and M3-O8, did not change with *P*.

As observed in several other silicates, the Si tetrahedra were unchanged, at least in the *P* range examined. The differences in average distances were within 2σ.

The bulk moduli of the A1 and A2 coordination polyhedra are 1350(150) and 1000(120) kbar, respectively. These values compare well with those measured for Ca polyhedra in other phases: K_{CaO_6} in lawsonite is 1140 kbar (Comodi and Zanazzi 1996), and the bulk modulus of $^{[8]}$Ca in grossular is 1150 kbar (Hazen and Finger 1978).

Comparison of the three structural refinements also showed that because many coordination polyhedra are linked by corner sharing in the clinozoisite structure, particularly on the (010) plane, the whole deformation mechanism involves polyhedral tilting, as well as a decrease in polyhedron size.

Relating the strain ellipsoid to the crystal structure explains why the largest variation lies approximately along the [001] direction and the smallest along [100]. The epidote structure was described by Gottardi (1968) as formed of "building blocks" consisting of octahedral chains with tetrahedra on opposite sides (Fig. 4). The various ways in which these blocks can be connected result in the various structures of sorosilicates such as ilvaite, pumpellyite, lawsonite, etc. In the epidote structure, there is a closed sequence of building blocks along the *a* axis, whereas the blocks are linked by tetrahedral corner sharing along the *c* axis. Therefore, the structure is more easily deformed along the *c* axis, by means of variations in the Si1-O9-Si2 angle, which changed from 162.9° at 0.5 kbar to 158.1° at 42 kbar (Table 8).

The "building blocks" scheme adequately explains the greater compressibility of the *c* lattice parameter with respect to *a*. However, to understand the orientation of the strain ellipsoid in the structure, it is useful to analyze bond-length distributions. Figure 2 shows the (010) section of the strain ellipsoid and the projection of the epidote structure onto the (010) plane (modified from Gabe et al. 1973). The directions of Si1···Si2 and M1···Si1 correspond to those of the largest and smallest principal compression axes, β_3 and β_1, respectively. Along the β_3 direction, Si1···Si2 decreased from 3.216(2) Å at 0.5 kbar to 3.183(7) Å at 42 kbar as a result of tetrahedral tilting (Table 8), whereas along the β_1 direction no tilting between the Si1 tetrahedron and the M1 octahedron was observed, and the M1-O1 and Si1-O1 bond distances did not change significantly with *P* (Table 7).

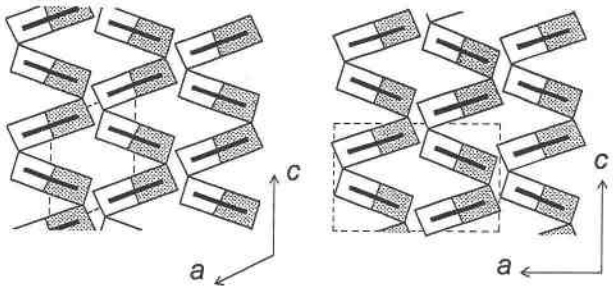

FIGURE 4. Structures of clinozoisite (**left**) and zoisite (**right**) projected along the *b* axis, represented with building blocks (modified from Gottardi 1968).

Temperature and pressure response of clinozoisite

T and *P* are often considered as analogous but opposite variables on the basis of thermodynamic and crystal-chemical evidence. Although inverse behavior is observed in many crystal structures (e.g., Hazen and Finger 1982, and references therein), a few examples indicate that a nearly perfect overlap exists between the deformations induced by *P* and *T*, as in epidote. In fact, comparison of our compression data for clinozoisite with the high-*T* data from the single-crystal refinement of a strontian piemontite (Catti et al. 1988) reveals not only the same orientation of the strain ellipsoid with both *P* and *T*, and its strong anisotropy, but also the same tetrahedral tilting. Thus, the Si1-O9-Si2 angle increases with *T* and decreases with *P*, and there is the same evolution of the individual polyhedral bond distances, with polyhedral distortion decreasing with *P* and increasing with *T*.

Thermal expansion coefficients for zoisite and clinozoisite were determined using a high-*T* powder diffractometer by Pawley et al. (1996). The values of α were $3.86(5) \times 10^{-5}$ and $2.94(5) \times 10^{-5}$ K^{-1}, respectively, for the two polymorphs. The latter value is in good agreement with that of Catti et al. (1988) for the strontian piemontite, $3.01(6) \times 10^{-5}$ K^{-1}.

A *P-T* gradient indicating the geometric stability of clinozoisite may therefore be proposed. Assuming that derivatives $\delta\alpha/\delta P$ and $\delta\beta/\delta T$ are zero, that the α_V value is 3.0×10^{-5} K^{-1}, and that the β_V value measured for clinozoisite is 7.7×10^{-4} $kbar^{-1}$, then the calculated α/β ratio is 38 bar/K. To a first approximation, this ratio compares well with that of 34 bar/K measured in lawsonite (Comodi and Zanazzi 1996). Both values are significantly higher than the average initial geothermal gradient, which is about 20 bar/K (Angel et al. 1988). Therefore, clinozoisite should remain stable, at least from a structural point of view, with geothermal gradients of about 10 °C/km, in good agreement with the results obtained from experimental petrology.

ACKNOWLEDGMENTS

We thank P. Bonazzi and S. Menchetti for kindly loaning the clinozoisite sample, and C. Cipriani for the zoisite sample from the Museum of Mineralogy of Florence University. Financial support was provided by MURST (40% and 60% funds) and CNR (grant no. 95.00372.CT05).

References cited

Ackermand, D., and Raase, P. (1973) Coexisting zoisite and clinozoisite in biotite schists from the Hohe Tauern, Austria. Contributions to Mineralogy and Petrology, 42, 333–341.

Angel, R.J., Hazen, R.M., McCormick, T.C., Prewitt, C.T., Smyth, J.R. (1988) Comparative compressibility of end-member feldspars. Physics and Chemistry of Minerals, 15, 313–318.

Bonazzi, P., and Menchetti, S. (1995) Monoclinic members of the epidote group: Effects of the $Al \leftrightarrow Fe^{3+} \leftrightarrow Fe^{2+}$ and of the entry of REE^{3+}. Mineralogy and Petrology, 53, 133–153.

Catti, M., Ferraris, G., and Ivaldi, G. (1988) Thermal behavior of the crystal structure of strontian piemontite. American Mineralogist, 73, 1370–1376.

Comodi, P., and Zanazzi, P.F. (1993) Improved calibration curve for the Sm^{2+}:BaFCl pressure sensor. Journal of Applied Crystallography, 26, 843–845.

Comodi, P., Melacci, P.T., Polidori, G., and Zanazzi, P.F. (1994) Trattamento del profilo di diffrazione da campioni in cella ad alta pressione. Proceedings of XXIV National Congress of Associazione Italiana di Cristallografia, Pavia, 27–29 September, 119–120.

Comodi, P., and Zanazzi, P.F. (1996) Effects of temperature and pressure on the structure of lawsonite. American Mineralogist, 81, 833–841.

Denner, W., Schulz, H., and d'Amour, H. (1978) A new measuring procedure for data collection with a high-pressure cell on X-ray four-circle diffractometer. Journal of Applied Crystallography, 11, 260–264.

Dollase, W.A. (1968) Refinement and comparison of the structures of zoisite and clinozoisite. American Mineralogist, 53, 1882–1898.

Finger, L.W., and King, H. (1978) A revised method of operation of the single-crystal diamond cell and refinement of the structure of NaCl at 32 kbar. American Mineralogist, 63, 337–342.

Gabe, E.J., Portheine, J.C., and Whitlow, S.H. (1973) A reinvestigation of the epidote structure: Confirmation of the iron location. American Mineralogist, 58, 218–223.

Glinnemann, J. (1990) Future prospects of laboratory diamond-anvil-cell work. Abstracts of the XVth Congress I.U.Cr., Bordeaux, France, July 19–28, C-354.

Gottardi, G. (1968) Structural features of some group-silicates with chain of octahedra. Tschermaks für Mineralogische und Petrographische Mitteilungen, 12, 129–139.

Hazen, R.M., and Finger, L.W. (1978) Crystal structures and compressibilities of pyrope and grossular to 60 kbar. American Mineralogist, 63, 297–303.

——— (1982) Comparative crystal chemistry, 231 p. Wiley, New York.

Holland, T.J.B., Redfern, S.A.T., and Pawley, A.R. (1996) Volume behavior of hydrous minerals at high pressure and temperature: II. Compressibilities of lawsonite, zoisite, clinozoisite, and epidote. American Mineralogist, 81, 341–348.

Ito, T. (1950) X-ray studies on polymorphism. Maruzen, Tokyo, 50–69 (quoted in Structure Reports, 13, 375–376).

Jenkins, D.M., Newton, R.C., and Goldsmith J.R. (1983) Fe-free clinozoisite stability relative to zoisite. Nature, 304, 622–623.

Kvick, A., Pluth, J.J., Richardson, J.W., Jr., and Smith, J.V. (1988) The ferric ion distribution and hydrogen bonding in epidote: A neutron diffraction study at 15 K. Acta Crystallographica, B44, 351–355.

North, A.C.T., Phillips, D.C., and Mathews, F.S. (1968) A semiempirical method of absorption correction. Acta Crystallographica, A24, 351–359.

Ohashi, Y. (1982) A program to calculate the strain tensor from two sets of unit-cell parameters. In R.M. Hazen and L.W. Finger, Comparative crystal chemistry, p. 92–102. Wiley, New York.

Pawley, A.R., and Wood, B.J. (1995) The high-pressure stability of talc and 10 Å phase: Potential storage sites for H_2O in subduction zones. American Mineralogist, 80, 998–1003.

Pawley, A.R., Redfern, S.A.T., and Holland, T.J.B. (1996) Volume behavior of hydrous minerals at high pressure and temperature: I. Thermal expansion of lawsonite, zoisite, clinozoisite, and diaspore. American Mineralogist, 81, 335–340.

Poli, S., and Schmidt, M.W. (1995) H_2O transport and release in subduction zones: Experimental constraints on basaltic and andesitic systems. Journal of Geophysical Research, 100, 22299–22314.

Prunier, A.R., Jr., and Hewitt, D.A. (1985) Experimental observations on coexisting zoisite-clinozoisite. American Mineralogist, 70, 375–378.

Ray, N.Y., Putnis, A., and Gillet, P. (1986) Polytypic relationship between clinozoisite and zoisite. Bulletin de Minéralogie, 109, 667–685.

Reynard, B., Fiquet, G., Itié, J.-P., and Rubie, D.C. (1996) High-pressure X-ray diffraction study and equation of state of $MgSiO_3$ ilmenite. American Mineralogist, 81, 45–50.

Ross II, C.R., and Webb, S.L. (1990) BIRCH, a program for fitting *PV* data to an Eulerian finite-strain equation of state. Journal of Applied Crystallography, 23, 439–440.

Schlenker, J.L., Gibbs, G.V., and Boisen, M.B., Jr. (1978) Strain-tensor components expressed in terms of lattice parameters. Acta Crystallographica, A34, 52–54.

Schmidt, M.W., and Poli, S. (1994) The stability of lawsonite and zoisite at high pressures: Experiments in CASH to 92 kbar and implications for the presence of hydrous phases in subducted lithosphere. Earth and Planetary Science Letters, 124, 105–118.

Schreyer, W.E. (1988) Experimental studies on metamorphism of crystal rocks under mantle pressures. Mineralogical Magazine, 52, 1–26.

Shannon, R.D. (1976) Revised effective ionic radii and systematic studies of interatomic distances in halides and chalcogenides. Acta Crystallographica, A32, 751–767.

Sheldrick, G.M. (1976) SHELX-76. Program for crystal structure determination. University of Cambridge, Cambridge, England.

Ulmer, P., Trommsdorff, V., and Reusser, E. (1994) Experimental investigation of antigorite stability to 80 kbar. Mineralogical Magazine, 58A, 918–919.

Manuscript received April 1, 1996
Manuscript accepted September 20, 1996